Metallurgical and Materials Engineering *Research paper*
https://doi.org/10.56801/MME867

EFFECT OF FEEDING FLOW RATE ON CHARACTERISTICS OF $CuInSe_2$ FILMS PREPARED BY FLASH EVAPORATION

Abdelwahab Hamdi[1], Ali Cheknane[1], Hikmat S. Hilal[2]*

[1]Laboratoire Matériaux, systèmes énergétiques, énergies renouvelables et gestion de l'énergie. Université Amar Telidji de Laghouat. Bd des Martyrs BP37G, Laghouat-03000- Algérie
[2]SSERL, Department of Chemistry, An-Najah National University, Nablus, Palestine

Received 18.07.2022
Accepted 26.12.2022

Abstract

Copper indium selenide $CuInSe_2$ (CISe) is one of the most promising absorber materials in high efficiency heterojunction thin-film solar cells due to its high conversion efficiency and known high stability. This paper describes a simple method for preparing $CuInSe_2$ films from pre-prepared $CuInSe_2$ ingot powder using a flash evaporation method. The primary goal of this work is to investigate the effect of feeding flow rate on $CuInSe_2$ film characteristics. The powder feeding flow rate into the evaporator has been adjusted to control the film growth rate. Structure, composition, morphology, electrical and optical properties have all been studied for films deposited at different feeding flow rates. The results show that varying the feeding flow rate affects film characteristics, and that lower feeding rates yield films with better characteristics, which should be considered in future semiconductor film processing.

Keywords: $CuInSe_2$; Photovoltaics; Chalcopyrite; Absorber layer; Feeding flow rate in flash evaporation.

Introduction

Since their discovery in 1953 by Hann and colleagues, the I-III-VI2 type ternary chalcopyrite compounds have quickly gained prominence in optoelectronic applications, particularly in photovoltaics. $CuInSe_2$ (CISe) [1] is one such material, with a direct band gap of 1.04 eV [2] and an optical absorption coefficient of 105 cm^{-1}, which is twice that of Si [3]. The material is a promising candidate for multi-layer solar cells due to its high conversion efficiency of more than 16% [1]. Solar cells based on $CuInSe_2$ have good chemical stability and control doping [4]. $CuInSe_2$-based thin films are also useful absorber materials because their band gap values can be tuned between 1.018 and

*Corresponding authors: Ali Cheknane, *a.cheknane@lagh-univ.dz*

1.701 eV [5-6] by varying the ratios of Ga and/or Se. Because of their appealing optoelectronic properties, Se-based absorbers such as CISe, CIGSe, and CZTSe have received tremendous attention in photovoltaic technology [7].

Furthermore, $CuInSe_2$ has the advantage of being produced as thin films, either p- or n-types, allowing for the low-cost production of a wide range of homo and hetero-junction components [8]. The electronic affinity and lattice parameters are also compatible with CdS semiconductor, which has a larger direct band gap and a proven efficiency in solar cells [9].

There are several techniques to prepare $CuInSe_2$ thin films. Examples are: thermo-reactive deposition (TRD), chemical vapor deposition (CVD) [10], electroplating [11-13], reactive spray deposition (Spray) [8], vacuum thermal evaporation deposition [8], reactive cathode sputtering (Sputtering) [14] and others. Best results were reported using the vacuum thermal evaporation technique [15] where the preferred orientation (112) is generally obtained [16-18].

$CuInSe_2$ film research is still ongoing, with the goal of optimizing its properties for solar cell and infrared device applications. *Mobarak et al.* recently investigated the growth method on $CuInSe_2$ bulk crystal characteristics [19]. *Weng et al.* used the Bridgman method to create single crystals of $CuInSe_2$ [20]. *Wada et al.* [21], *Klenk et al.* [22], and others have reported on the PVD growth of $CuInSe_2$ films. $CuInSe_2$ films electrochemically deposited have also been reported [23-25]. *Kim et al.* reported the deposition of $CuInSe_2$ films for near-infrared photodetector applications, and they tuned their properties by varying the Cu/In ratio [3]. *Palmiotti et al.* studied the effect of Na_2O on the film growth rate and crystallite quality of amorphous $CuInSe_2$ films deposited on soda lime glass and silicon substrates [26]. Researchers reported on $CuInSe_2$ films from various perspectives, including method or preparation, substrate impact, preparation conditions, and characteristic tuning. To our knowledge, the effect of ingot powder feeding flow rate on prepared $CuInSe_2$ film properties has not been reported, particularly in the flash evaporation method.

The purpose of this research is to control the ingot powder feeding flow rate during film preparation to control the structural, morphological, electrical, and optical properties of $CuInSe_2$ films. The flash evaporation technique was used here, which involves evaporating the three elements (Cu, In, Se) from a single source. This was accomplished by feeding a boat (crucible) at various flow rates with a $CuInSe_2$ ingot powder inside at a high temperature of 1500 ℃. To the best of our knowledge, no similar studies were reported prior.

Experimental

Materials and equipment

The starting materials Cu (Merck Model No. 203122, 99.999%), In (Merck Model No. 203432, 99.999%) and Se (Merck Model No. 229865, 99.99%) have been purchased in their pure elemental powder forms from Sigma-Aldrich. The ingot was created using a special quartz ampoule, which is described further below. A muffle furnace was used to heat the ingots during the preparation process. The films were made with a flash evaporation system, as described below. As a target (source of evaporation), a commercial tungsten boat was heated to the desired temperature (1500 ℃). A commercial SiO_2 substrate (Corning Sigma-Aldrich Model No CLS294775X25) was cut to 15x25x1 mm^{-3}

dimensions and placed 7 cm away from the target, as described below. At 300 °C, the substrate was heated by electrical resistance. The tungsten boat was fed with ingot powder at various feeding flow rates until all of the powder (520 mg) was added. The addition time has been varied between 13 and 25 minutes.

On a Philips type X'pert equipment, X-ray diffraction (XRD) patterns were measured. For the entire XRD pattern, Rietveld analysis with FullProf software was used. SEM images were captured using a Hitachi S2500C thermal-field emission gun scanning electron microscope, a Thermo Scientific Quattro SEM, and a VEGA3 TESCAN equipped with energy-dispersive X-ray (EDX) spectroscopy. A Dfp-03 four-point probe device was used to measure electrical properties. Transmittance spectra in the UV, visible, and near infrared ranges were recorded using a JASCO type spectrometer (190 nm to 2500 nm). The spectrometer has two detectors: a photomultiplier for ultraviolet/visible and a lead sulfide detector for near infrared.

Ingot processing

A $CuInSe_2$ ingot was prepared and ground into powder prior to film deposition. The ingot was made with a cylindrical quartz tube with an inside diameter of 13 mm, shaped like a bulb with one end rounded. Figure 1 shows how the tube is welded to another quartz tube with an inside diameter of 5 mm and a length of 30 cm. The bulb was rinsed with distilled water, degreased with acetone, and then treated for 30 minutes with a solution of HF, HNO_3, and H_2O. It was then thoroughly rinsed with distilled water once more. The bulb was then carefully dried in a 450 °C furnace for 4 hours.

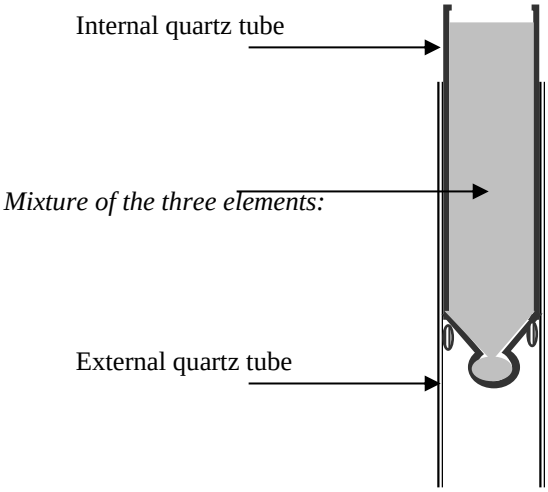

Fig. 1. Bulb used for ingot synthesis

The elements Cu, In and Se have been accurately weighed in a four-digit balance to have a mixture of mole ratio 1:1:2, respectively. The mixture has been thoroughly mixed, ground in a mortar under dry conditions, placed inside the quartz bulb, evacuated at 6.67×10^{-6} mbar (6.67×10^{-4} Pa) and sealed. The ampoule has then been placed inside a furnace. The temperature has been gradually increased from room temperature to 410 °C

in the course of 2 hours. Heating has then been increased to 1010 ºC. To ensure powder homogeneity during heating, the contents of the ampoule have been stirred by shaking the support that holds the bulb. Heating and shaking have been continued for 8 hours at a carefully controlled temperature of 1010 ºC. The furnace was then turned off to allow it to cool to room temperature before the bulb was carefully broken to accept the resulting polycrystalline ingot. To prepare it for characterization, the ingot has been tailed and polished.

Polycrystalline growth on the tip of the ingot was observed prior to grinding. However, the presence of an outgrowth at the end confirms the formation of a single large crystal within the ingot. Many vacancies and small single crystals were discovered after longitudinally cutting the ingot into four pieces. The Hot-Probe technique was used to determine the conduction type of ingot in order to determine the type of semiconductor. The results obtained with the aforementioned technique show that all four pieces of the ingot are of type n conduction.

The ingot has then been crushed, ground and sieved to obtain a homogeneous powder with a size of 2 to 10 µm. This has been confirmed by SEM image, Figure 2. All Cu, In and Se elements are confirmed by the EDX spectra in the Figure. The EDX spectrum confirms the purity of the ingot powder as no foreign elements can be observed.

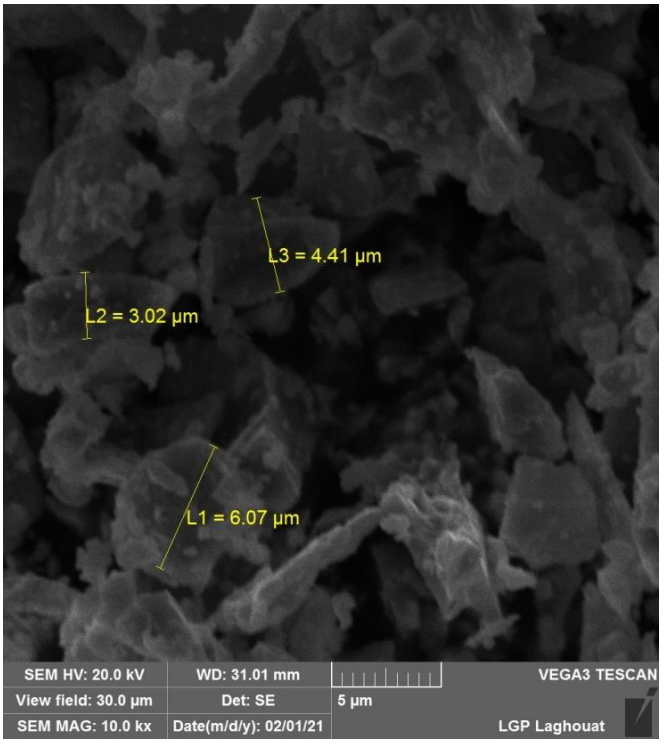

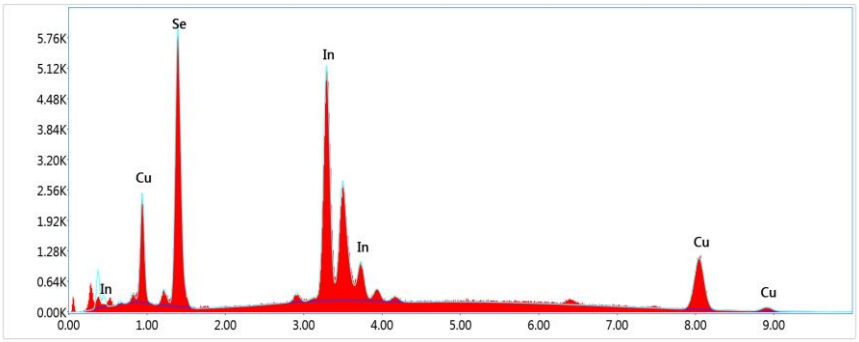

Fig. 2. SEM image measured for $CuInSe_2$ ingot powder, together with EDX spectrum.

Table 1. EDX values measured for $CuInSe_2$ ingot powder

Element	*Weight %*	*Atomic%*	*Error%*	*Net Int.*	*R*	*A*	*F*
Cu K	19.32	28.85	4.34	344.79	0.8186	0.8477	1.1038
Se K	11.93	14.33	5.34	96.65	0.8501	0.9158	1.1882
In L	68.75	56.82	5.16	1028.79	0.7715	0.6187	1.0063

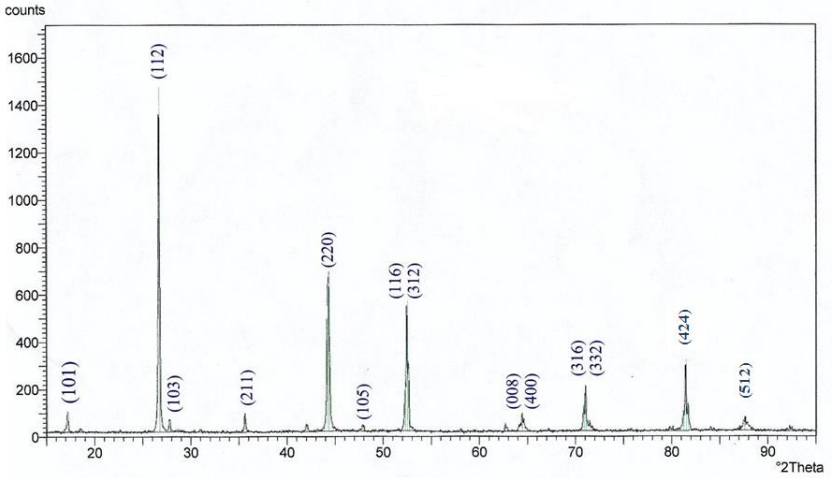

Fig. 3. RXD pattern measured for the $CuInSe_2$ ingot powder.

Crystal structure for the ingot powder has been studied by XRD, Figure 3. The XRD pattern shows a series of lines with varying intensities and shapes. The reflections (101) at 2θ = 17.1º, (112) at 26.6 º, (103) at 27.7º, (211) at 35.7º (220) at 44.2°, (116) at

52.2°, (312) at 52.4°, (008) at 64°, (213) at 41.9 º, (400) at 64.3°, (316) at 70.7°, (332) at 71º, (424) at 81.4° and 87.5° confirm the $CuInSe_2$ compound in a chalcopyrite phase, as reported earlier [3, 27-32]. The reflection 18 is not considered by FullProf software.

$CuInSe_2$ film preparation

The primary goal of this study is to determine the effect of powder feeding flow rate on $CuInSe_2$ film characteristics using the flash evaporation technique. A special device, as shown in Figure 4, has been used for this purpose. The device consists of a tungsten boat (evaporation source) that can be fed $CuInSe_2$ powder at variable feeding flow rates. Other parameters, such as the distance between the source of evaporation and the substrate at 7 cm, the substrate temperature at 350 ºC, the boat temperature at 1500 ºC, and the working pressure at $8x10^{-6}$ -$7x10^{-6}$ mbar, have remained constant throughout the various film preparations ($8x10^{-4}$ – $7x10^{-4}$ Pa).

To achieve a high vacuum of $2x10^{-6}$ to $1x10^{-6}$ mbar ($2x10^{-4}$–$1x10^{-4}$ Pa), the substrate has been slowly heated for at least 15 min. The substrate was exposed inside the system under vacuum once the temperature reached 300 ºC. The boat was also heated during the degassing process, and the substrate cover was placed beneath the boat because its surface may contain an oxide layer that could contaminate the deposits. Evaporation was carried out under the aforementioned conditions with varying ingot powder feeding flow rates. After the evaporation process was completed, the power supply to the boat and the flash device was turned off, keeping the system under vacuum. To anneal under vacuum, the film/substrate temperature was gradually lowered (over 45 minutes). Profilometry measured the thicknesses of films deposited at various feeding flow rates to be 100 nm, which is equivalent to a total mass of 2.25 mg for the produced film.

In case of preparation at high $CuInSe_2$ powder feeding flow rates (30 or 40 mg/min) with boat temperatures ~1500 °C, some grains fell onto the boat and then directly sublimed. That indicates increased vapor pressure during evaporation. In preparations at lower feeding flow rates, no additional grains occurred onto the boat.

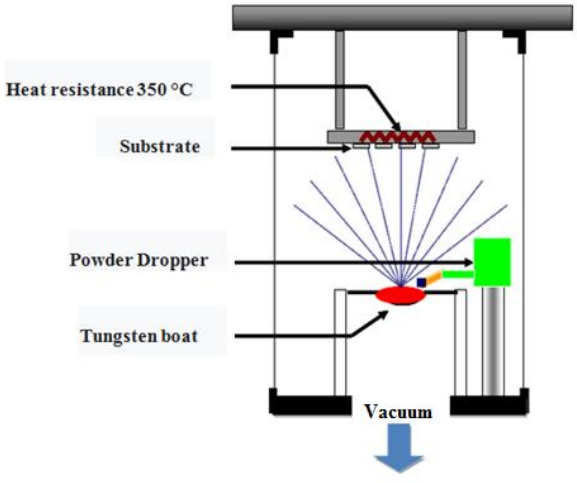

Fig. 4. Schematic showing the flash evaporation device used to prepare $CuInSe_2$ films.

Results

The $CuInSe_2$ films, prepared at various powder feeding flow rates, have been studied by various methods including XRD for structure, SEM micrographs for morphology, EDX spectra for composition, electrical properties and optical properties, as described here.

Film XRD patterns

XRD patterns have been measured for $CuInSe_2$ films prepared at various feeding flow rates of powder injection in the evaporator as shown in Figure 5. In all films, the main reflection corresponds to orientation (112) which means that the $CuInSe_2$ phase exists in all cases.

In case of high feeding flow rate, 40 and 22 mg/min, a secondary reflection that corresponds to $Cu_2In_4Se_7$ compound [33] can be observed at $2\theta=21.5^o$. The corresponding reflection height is larger for the rate 40 mg/min than the 22 mg/min. At lower rates, 20 mg/min or lower, the reflection cannot be clearly observed. The reflection indicates excessive presence of selenium element in the films.

The reflection at $2\theta=25^o$ that corresponds to In_2Se_3can be observed for higher feeding flow rates 40 and 22 mg/min. In case of lower flow rates, the reflection cannot be clearly observed. The XRD patterns thus show the production of $Cu_2In_4Se_7$ and In_2Se_3 phases at higher powder flow rates only.

The secondary reflection (101) at $2\theta=16.5^o$, which corresponds to the $CuInSe_2$ phase, can be observed for all feeding flow rates. Unlike $Cu_2In_4Se_7$ and In_2Se_3 phases, the results confirm the production of $CuInSe_2$ at all flow rates. The results will be discussed in Section 4.

Values of crystallite sizes for various films are calculated based on the Scherrer equation, and are shown in Table 2. The Table shows that the crystallite size is smaller in films prepared at lower flow rates. Based on XRD results, high flow rate preparations are those performed at higher than 20 mg/min, while low flow rate preparations are those performed at 20 mg/min or lower.

Table 2. Crystallite size average values calculated using the Scherrer equation, for films deposited at various flow rates.

Feeding flow rate (mg/min)	Crystallite size D (nm)
20	50.77
30	47.69
40	42.42

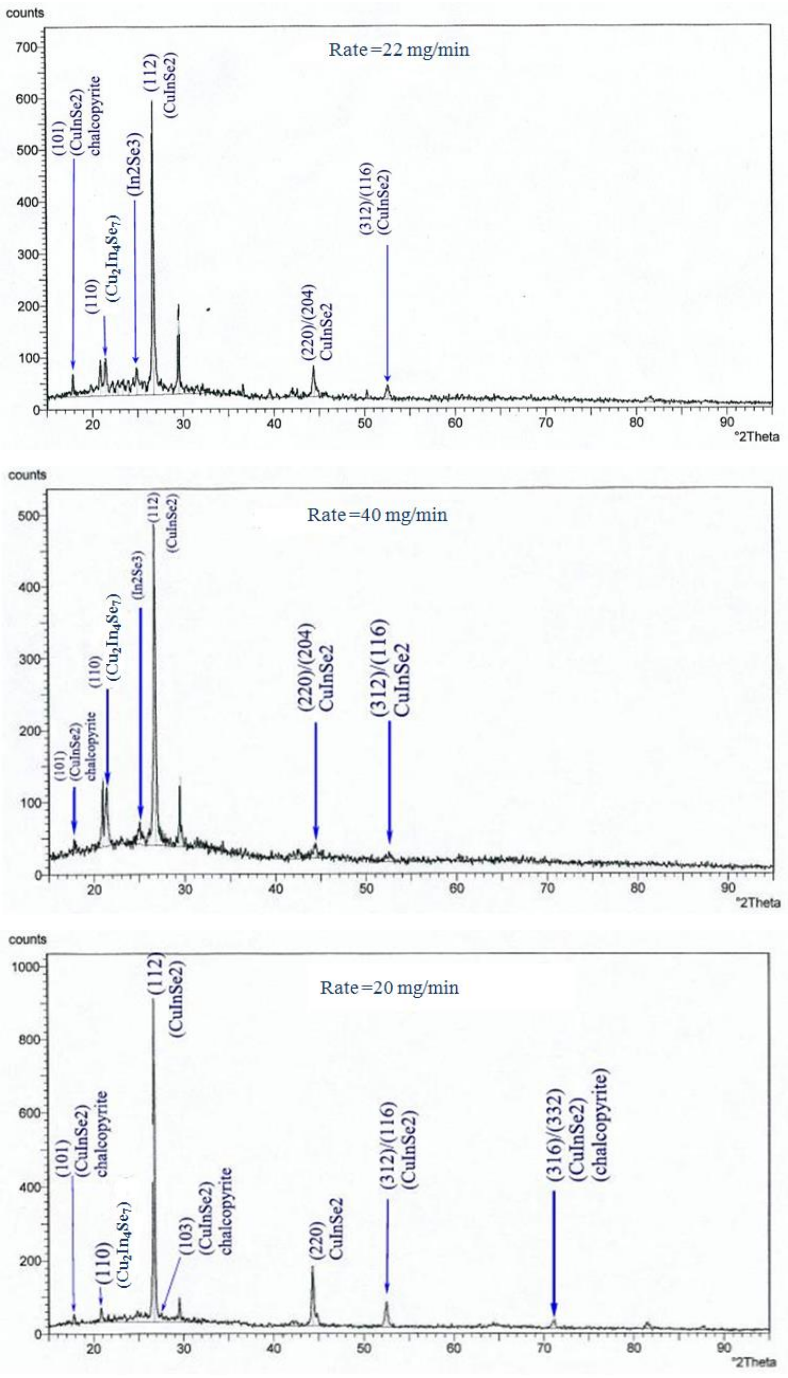

Fig. 5. XRD patterns measured for $CuInSe_2$ films prepared at various feeding flow rates.

Film morphologies at various feeding flow rates

The morphologies for various $CuInSe_2$ films prepared at two different feeding flow rates, namely 40 mg/min (as example for high rate) and 20 mg/min (as example for lower rates) have been studied using SEM micrographs. Figures 6 and 7 summarize the SEM images measured for cross-sectional and surface.

In surface SEM images, Figure 6, the films prepared at high feeding flow rates have additional spheres at the surface. These spheres are due to the secondary phases $Cu_2In_4Se_7$ and In_2Se_3 observed by XRD. At lower flow rate, the film appears more uniform and compact with no clear extra spheres. This behavior will be further discussed in the next Section. The SEM images show uniform agglomerates of sizes ~94 nm for the 20 mg/min flow rate, while the film prepared at 40 mg/min shows non-uniform agglomerates of larger sizes. Combined together, the results indicate that the larger agglomerates (observed by SEM) involve smaller crystallites (observed by SEM).

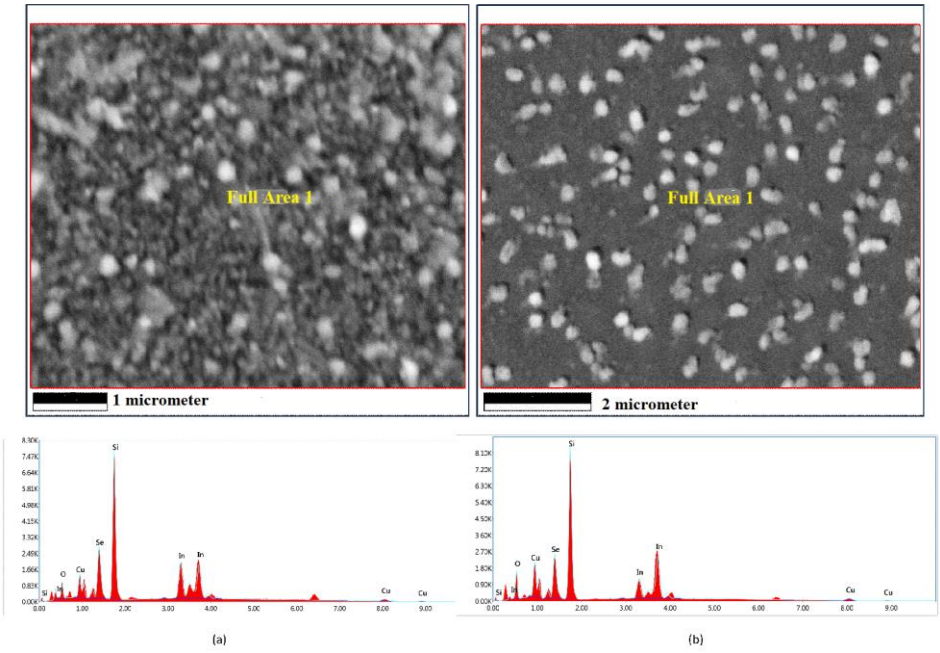

Fig. 6. SEM images and EDX spectra measured for $CuInSe_2$ films prepared at various powder feeding flow rates. (a) low at 20 mg/min and (b) high at 40 mg/min.

The cross-sectional SEM micrograph has been measured for $CuInSe_2$ film prepared at 20 mg/min Figure 7. The Figure indicates a columnar structure with ~100 nm thickness.

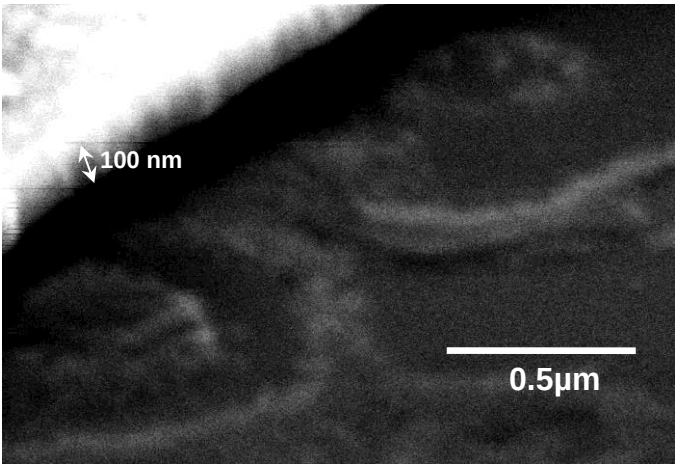

Fig. 7. Cross-sectional SEM image for $CuInSe_2$ film prepared 20 mg/min.

The EDX spectra shown in Figure 6 are summarized in Table 3. Atomic percentage values for Cu, In and Se are observed. In both films, Si and O have high atomic percentage values. Both elements exist in the substrate and should be observed in each film. Table 3 shows no foreign elements in the film. However, the atomic percentage values are not conclusive and do not show the atomic ratios of elements present in the substrates or the films. For instance, the substrate which is SiO_2, should have Si to O atomic ratio 1:2, cannot be observed in Table 3. Moreover, the expected atomic ratios 1:1:2 for $CuInSe_2$ films cannot be observed. However, Table 3 confirms the existence of elements Si, O, Cu, In and Se with a total atomic percentage of nearly 100%.

Table 3. EDX values for $CuInSe_2$ films prepared at various feeding flow rates. (a) 20 mg/min, and (b) 40 mg/min.

(a)

Element	Weight%	Atomic %	Error%	Net Int.	R	A	F
O K	28.05	50.22	12.61	93.02	0.8424	0.0377	1.0000
Si K	40.50	41.30	7.58	1199.87	0.8721	0.3537	1.0064
Cu K	2.05	0.92	9.71	36.86	0.9251	0.9169	1.1177
Se K	1.96	0.71	9.99	16.16	0.9418	0.9665	1.2603
In L	27.44	6.85	5.37	389.30	0.8939	0.6315	1.0043

(b)

Element	Weight%	Atomic%	Error %	Net Int.	R	A	F
O K	38.61	58.96	11.49	159.30	0.8697	0.0486	1.0000
Si K	41.68	36.25	7.21	1300.91	0.8967	0.3873	1.0049
Cu K	2.68	1.03	7.86	47.35	0.9425	0.9385	1.1184
Se K	1.39	0.43	12.16	11.09	0.9562	0.9747	1.2642
In L	15.64	3.33	5.32	218.26	0.9159	0.6457	1.0043

Electrical properties

The doping concentration (Nd) is traditionally determined using the four-point probe method and eddy current mapping [34-35]. The four-point probe technique is used to determine resistivity here, while the hot point technique is used to determine the type of majority carriers for each produced layer. Table 4 summarizes the electrical resistivity values for 100 nm thick films prepared at feeding flow rates of 20, 30, and 40 mg/min. According to Table 4, the film resistivity is lower for films prepared at a lower powder feeding flow rate. Furthermore, the hot peak measurement revealed that all prepared films use p-type conduction. All of the outcomes are discussed further below.

Table 4. Effect of powder feeding flow rate on square resistance values for $CuInSe_2$ films

	Feeding flow rate (mg/min)		
	20	30	40
Resistivityρ (Ω.cm)	$2.45x10^{-3}$	$1.86x10^{-2}$	$6.37x10^{-2}$

Optical characteristics

This paper investigates the effect of powder feeding flow rate on film optical properties. The transmission spectra and optical absorption coefficients of films prepared at flow rates of 20, 30, and 40 mg/min have been plotted.

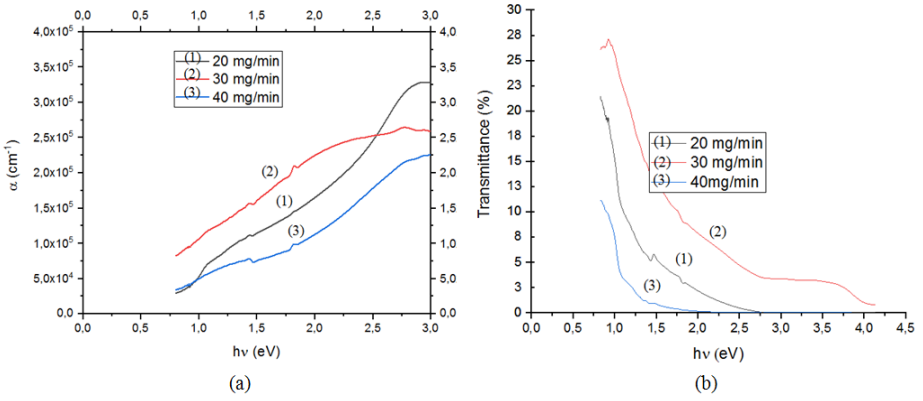

Fig. 8. Optical characteristics measured for $CuInSe_2$ films prepared at various powder feeding flow rates. (a) Absorption coefficient (cm^{-1}) and(b) Transmittance (%).

The results of absorption coefficient and transmittance spectra measurements at room temperature for various 100 nm thick films are summarized in Figure 8. According to the transmittance spectra (Figure 8a), the film prepared at 30 mg/min has the highest transmittance over a wide range of 300-1400 nm (0.88 to 4.1 eV). The film prepared at 20 mg/min has a lower transmittance in the same range. The film prepared at 40 mg/min has a lower transmittance within the range (1.0-4.1 eV), which corresponds to (300-1200 nm), but a higher transmittance after that compared to other two counterpart films. Figure 8a shows that for wavelengths of 2.5 eV (500 nm) and shorter, the film prepared at 20 mg/min has the highest absorption coefficient of the series.

Discussion

XRD pattern in Figure 3 confirms the production of $CuInSe_2$ ingot as desired. The ingot composition is consistent with the nominal amounts of used elements in the ingot preparation, as the ampoule is closed, no elements can be added or lost during heating. As described above, the XRD pattern shows all possible reflections for the $CuInSe_2$ phase only with no possibility for $Cu_2In_4Se_7$ or In_2Se_3phases.

For $CuInSe_2$ films, the XRD patterns vary with powder feeding flow rate. At higher flow rates, the two species $Cu_2In_4Se_7$ and In_2Se_3 can be observed. The results can be justified by the mechanisms proposed earlier [36]. By heating the $CuInSe_2$, it degrades as shown in equation (1):

$$4CuInSe_{2(s)} \rightarrow 4Cu_{(s)} + 2In_2Se_{(g)} + 3Se_{2(g)} \qquad 1$$

In case of high feeding flow rate preparations, the gas species would be carried away readily before the resulting copper metal evaporates. This leaves the resulting film in partial deficiency of copper, where the two additional phases In_2Se_3 and $CuInSe_3$ appear. On the other hand, in case of low flow rate preparation, there will be enough time for the solid copper element to evaporate and catch up with the $CuInSe_2$ film build up, leaving no chance for the additional two phases to appear. The production of Cu metal upon heating $CuInSe_2$ ingots has also been documented earlier [37]. The results are consistent with earlier report that described how Cu concentration affects the $CuInSe_2$ crystal structure [38].

The same logic can be used to explain film SEM images and morphologies. The product involves more than one phase at higher flow rates, which affects the film morphology. This is due to copper atom loss during evaporation and condensation. Films made at lower flow rates only involve one phase of $CuInSe_2$. The morphology differences between the various preparations are most likely due to differences in phase purity. Previously published research indicated that mixed phase semiconductor materials may have different properties than mono-phase films [39-40].

The EDX results show that there are no foreign elements in the ingot powder or the films. The measured Cu:In:Se atomic ratios, however, are inconsistent with the $CuInSe_2$ phase. Table 3 shows the presence of excess elemental Cu and In phases in the films. This is consistent with previous discussions based on Equation (1).

Table 1 also shows excess Cu and In metal phases that could be produced by Equation (1). Unreacted materials may also produce excess Cu and In elemental phases. Table 1 shows that the Se element has a lower atomic ratio than the Cu and In elements. The Se element, with a relatively low boiling point of 685 ℃, may escape under the heating and evacuation conditions described in Section 2. 2.

As shown in Table 4, the feeding flow rate influences the electrical properties of the film, with lower rate films having lower resistivity. The XRD and morphology discussions above explain this. Lower flow rates result in mono-phase films with greater uniformity and compactness. This helps to explain why lower flow rate preparation yields lower resistivity films.

Figure 8a shows that the absorption coefficient values for the film prepared at a lower flow rate are higher than those for other counterparts in the 500 nm or shorter range. This demonstrates the film's utility in solar cells with visible regions. The films are also

useful in infrared region applications, as described in Section 1 above, due to their low band gap value of 1.04 eV, which corresponds to 1200 nm.

Overall, when all characteristics of prepared films are considered, the film prepared at the lower flow rate exhibits the best characteristics. As a result, the lower feeding rate should be considered when preparing $CuInSe_2$ films for various applications.

Conclusion

$CuInSe_2$ films were prepared by the flash evaporation method. $CuInSe_2$ ingot was first prepared, characterized and ground to powder. The powder was fed into the flash evaporator at various feeding flow rates. The resulting films were characterized by various methods including XRD, SEM, electrical and optical properties. Films prepared at higher flow rates involved additional phases of $Cu_2In_4Se_7$ and In_2Se_3. Lower flow rate films showed highest $CuInSe_2$ phase purity, highest uniformity, lowest resistance and highest absorption coefficient (at ~500 nm or shorter), and soundly medium transmittance value. Based on the results, it is advisable to prepare $CuInSe_2$ films at lower powder feeding flow rates.

Acknowledgement

A.C. and A.H. acknowledge financial support from Université Amar Telidji de Laghouat and the General Directorate of Scientific Research and Technological Development (DGRSDT), ALGERIA.

References

[1] Y. Poissant, Study and optimization of photovoltaic solar cells in polymorphous silicon thin layers, PhD Thesis -UMR 7647 du CNRS, Ecole polytechnique de France 2001

[2] J.E. Jaffe, A. Zunger: Phys Rev B, 29 (1984) 1882-1906.

[3] S-T. Kim, J-S. Yoo, M-W. Lee, J-W. Jung, J.-H. Jang: Appl Sci, 12 (2022) 92-99

[4] PS. Suryavanshi, H. Khunt, B. Rehani, CJ. Panchal: Mat Today Proc 4 (2017) 12500 –12504

[5] A. Bouich, B. Hartiti, S. Ullah, M. EbnTouhami, B. Mari, DMF Santos: Mat Today Proc 13 (2019) 663–669

[6] CD. Chien, FY. Cheng, CW. Chia, HL. Wen, LC. Yen: Int J Photoenergy. (2013) 905271- 905277.

[7] MR Pavallo. AN. Banerjee, VRM Reddy, SW. Joo, HR Barai, C. Park: Sol. Energy 208 (2020) 1001–1030.

[8] K. Belaghit, Fabrication and characterization of n-$CuInSe_2$ and ZnO materials obtained by reactive chemical spraying: Applications to solar photocells, PhD Thesis, Université de Montpellier II, France, 1991.

[9] JI. Contreras-Rascón, J. Díaz-Reyes, A. Flores-Pacheco, R. Lozada Morales, ME. Álvarez-Ramos, JA. Balderas-López: Results Phys., 22 (2021) 103914.

[10] Y. Matamura, T. Ikenoue, M. Miyake,T. Hirato: J Crys Growth, 548 (2020) 125862.

[11] M. Lindberg, P. Poulsen, P. Moller, in: Proceedings of the 14th Workshop on Quantum Solar Energy Conversion" Quantsol March 17-23, Rauris, Salzburg, Austria, European Society for Quantum Solar Energy Conversion 2002.

[12] S. Strehle, S. Menzel, JW. Barth, K. Wetzig: MicroelectEng, 87 (2010) 180-186.

[13] L. Zhao, S. Yu, X. Li, M. Wu, L. Li: Sol Energy Mat Sol. Cells, 201 (2019) 110067.

[14] T. Yamaguchi, J. Matsufusa, A. Yoshida: Sol Energy Mat Sol. Cells. 27 (1992) 25-35**.**

[15] AN. Tuama, KH. Abass, MA. Bin Agam: Optik, 247(2021) 167980.

[16] JR. Tuttle, D. Albin, RJ. Matson, R. Noufi: J Appl Phys 66 (1998) 4408-4415.

[17] K. Konan, JK. Saraka, JT. Zoueu, P. Gbaha: J Appl Sci, 7 (2007) 478-483.

[18] ER. Don, R. Hill and GJ. Russel: Sol. Cells, 16 **(**1986**)** 131-142**.**

[19] M. Mobarak, MA. Zied, M. Mostafa, M. Ashari:, Heliyon, 6 (2020) e03196.

[20] WS. Weng, LS. Yip, I. Shihand, CH. Champness: Canad J Phys, 67 (1989) 294–297.

[21] T. Wada, N. Kohara, T. Negami, M. Nishitani: J Mat Res, 12 (1997) 1456–1462.

[22] R. Klenk, T. Walter, H.-W. Schock , D. Cahen: Adv Mat, 5 (1993) 114–119.

[23] YHL. Ribeiro, DGF. David, MVS. da Silvaand, ZN. da Rocha: Braz J Phys, 51(2021) 406–419.

[24] D. Prasher, T. Chandel, P. Rajaram: Electrochemical growth and studies of $CuInSe_2$thin films. Mat Res Exp, 1 (2014) 026401.

[25] Y-S. Cheng, W-R. Dai, M-P. Houng, in: 2017 IEEE International Conference on Applied System Innovation (ICASI), Sapporo, Japan, eds: Meen, T-H., Lam, ADK-T., Prior, ST. Institute of Electrical and Electronics EngineersInc, 2017, p 1367.

[26] E. Palmiotti, B. Belfore, D. Poudel, S. Marsillac, A. Rockett: Thin Solid Films, 746 (2022) 139095.

[27] A. Axelevitch, G. Golan: Series: Electron Energ 26 (2013) 187–195.

[28] S. Nithiananth, K. Silambarasan, T. Logu, S. Harish, R. Ramesh, C. Muthamizhchelvan, M. Shimomura, J. Archana, M. Navaneethan: Mat Lett, 308 (2022) 130887.
[29] A. Cho, SJ. Ahn, JH. Yun, J. Gwak, SK. Ahn, KSH. Song, KH. Yoon: Sol Energy Mat Sol Cells, 109 (2013) 17-25.
[30] R. Niranjan, A. Banotra, N. Padha: J. Mat Sci: Mat Electron, 31 (2020) 3172–3183.
[31] EP. Zaretskaya, VF. Gremenok, V. Riede, W. Schmitz, K. Bente, VB. Zalesski, OV. Ermakov: J Phys Chem Solids, 64 (2003) 1989-1993.
[32] NM. Shah, JR. Ray, VA. Kheraj, MS. Desai, CJ. Panchal, B. Rehani: J Mat Sci, 44 (2009) 316-322.
[33] Berghole Mohamed, Fabrication and characterization of Cu(Ga,In)Te_2 thin films by flash evaporation, PhD Thesis, Montpellier II, France 1979.
[34] Schroder DK. Semiconductor Material and Device Characterization. 3rd edition, J. Wiley & Sons, Hoboken, NJ, USA, 2006.
[35] Q. Wang, C. Zhang, Y. Du, R. Liu, L. Tan, W. Liu: Results Phys, 16 (2020) 102939.
[36] Jin-Wen Chu, properties of copper indium diselenide and action in photoelectrochemical cells, PhD Thesis, University of New South Wales, Faculty of Science, Sydney, Australia, May 1991.
[37] Y-H. Cheng, Y-L. Soo, S. Huang: Jap J Appl Phys, 39. (2000)379-381.
[38] H. Peng, DT. Schoen, S. Meister, XF. Zhang, Y. Cui: J Am Chem Soc, 129 (2007) 34–35.
[39] DAH. Hanaor, G. Triani, CC. Sorrell: Surf. Coat Technol, 205 (2011) 3658-3664.
[40] R. Murshed, S. Bansal: Mater, 15 (2022) 899.